

Density-dependent clustering: I. Pulling back the curtains on motions of the BAO peak

Mark C. Neyrinck,^{1,2,3} István Szapudi,⁴ Nuala McCullagh,¹ Alex Szalay,³ Bridget Falck,⁵ Jie Wang⁶

¹ *Institute for Computational Cosmology, Department of Physics, Durham University, South Road, Durham DH1 3LE, UK*

² *Institut d'Astrophysique de Paris, 98 bis bd Arago, 75014; Sorbonne Universités, UPMC Univ Paris 6 et CNRS, UMR 7095, Paris, France*

³ *Department of Physics and Astronomy, The Johns Hopkins University, Baltimore, MD 21218, USA*

⁴ *Institute for Astronomy, University of Hawaii, 96822 Honolulu, HI, USA*

⁵ *Institute of Theoretical Astrophysics, University of Oslo, PO Box 1029 Blindern, N-0315, Oslo, Norway*

⁶ *National Astronomy Observatories, Chinese Academy of Science, Datun Road, Beijing, PR China*

21 October 2016

ABSTRACT

The most common statistic used to analyze large-scale structure surveys is the correlation function, or power spectrum. Here, we show how ‘slicing’ the correlation function on local density brings sensitivity to interesting non-Gaussian features in the large-scale structure, such as the expansion or contraction of baryon acoustic oscillations (BAO) according to the local density. The sliced correlation function measures the large-scale flows that smear out the BAO, instead of just correcting them as reconstruction algorithms do. Thus, we expect the sliced correlation function to be useful in constraining the growth factor, and modified gravity theories that involve the local density. We find that the full run of the BAO peak location with density is best revealed when slicing on a $\sim 40 h^{-1}$ Mpc filtered density. But slicing on a $\sim 100 h^{-1}$ Mpc filtered density may be most useful in distinguishing between underdense and overdense regions, whose BAO peaks are shifted by a substantial $\sim 5 h^{-1}$ Mpc at $z = 0$. We also introduce ‘curtain plots’ showing how local densities drive particle motions toward or away from each other over the course of an N -body simulation.

Key words: large-scale structure of Universe – cosmology: theory

1 INTRODUCTION

The initial density fluctuations in the Universe are consistent with being perfectly Gaussian (Planck Collaboration et al. 2014). This is an appealingly simple situation, not only physically, but statistically, since it makes the power spectrum (or its Fourier dual, the 2-point correlation function – we use these terms interchangeably) optimal for scientific analysis of fully linear-regime observations such as the cosmic microwave background. But cosmological density fields on non-linear scales have substantial non-Gaussianity. It is a major challenge to capture all of the scientifically-relevant information from observations of the large-scale structure of the Universe, both in principle, and in a form that enables easy analysis and understanding.

The power spectrum can still be measured from non-Gaussian fields, of course, and used to constrain cosmology, galaxy formation, or whatever the observations might depend on. But, applied to a non-Gaussian field, the power spectrum is a blunt tool, and can fail to capture the vast majority of Fisher information available in principle. Practically, this means drastically degraded parameter constraints. This is known as the information plateau: as non-linearly small scales are analyzed, error bars do not shrink as they would for a Gaussian field, due to high variance and covariance on

small scales (Rimes & Hamilton 2005, 2006; Neyrinck et al. 2006; Neyrinck & Szapudi 2007; Takada & Jain 2009; Takahashi et al. 2011; Carron & Neyrinck 2012; Carron & Szapudi 2014; Wolk et al. 2015; Repp et al. 2015).

The conventional approach to measure information beyond the power spectrum is to measure polyspectra, or higher-point correlations. But in the non-linear regime, the ‘full hierarchy’ of these fails to contain all statistical information. Carron (2011) showed that for a lognormal random field, the full information resides in the power spectrum of the log density, but at small scales, the full hierarchy of correlations can miss dramatic amounts of information. The dark-matter density field is only approximately lognormal, and initial information is lost in principle from the coarse-grained density field, e.g. in stream crossing. But the field seems close enough to lognormal that a logarithm renders the field nearly as suitable for analysis by the power spectrum as a Gaussian field would be, enhancing the information content in the power spectrum by orders of magnitude in an ideal measurement (Neyrinck et al. 2009).

Going to lower instead of higher order, the 1-point probability density function (PDF), essentially ‘counts in cells’, already can contain plentiful information absent from the N -point correlation hierarchy. A well-known example in large-scale structure of a 1-

point statistic that contains information not in the first few correlation functions (indeed, often not in the full hierarchy, although this was not pointed out at the time) is the void probability function (White 1979). Analyzing the full PDF instead of just its moments is essential for maximal information extraction from strong-tailed distributions like the lognormal, since the moments do not uniquely characterize it, as is well-known in statistics (Aitchison & Brown 1957; Coles & Jones 1991; Carron 2011). Jointly analyzing a field's 1-point PDF, together with its higher-point statistics after Gaussianization (Neyrinck 2014), could even reduce some effects of biasing (McCullagh et al. 2016). (Gaussianization here means applying a rank-preserving monotonic transformation to produce a Gaussian 1-point PDF.) Recent analyses of cosmological fields have included measurements of the 1-point PDF, containing information not in the power spectrum (Hill et al. 2014; Liu et al. 2016).

Measuring the baryon acoustic oscillation (BAO) feature requires going at least to 2 point statistics. The quantity carrying the full information at 2-point order is the 2-point PDF $f(\delta_1, \delta_2; r)$. We call the (over)density $\delta = \rho/\bar{\rho} - 1$ simply 'the density.' f is the joint PDF of densities δ_1 and δ_2 (symmetric in them) at points separated by a distance r . The usual correlation function is an integral (Eq. 1) over f 's two density arguments.

An example of the high information content of the 2-point PDF is that the correlation function of any function of the density can be constructed by integrating over it with different weights. But having 3 arguments already makes the 2-point PDF possibly prohibitively unwieldy, for a few reasons. One reason is the sheer difficulty of visualizing, understanding, and modeling it. Also, in a practical measurement, slicing into the data into 3 arguments reduces the signal-to-noise ratio (S/N) of each bin of (δ_1, δ_2, r) . That is even assuming that the covariance matrix, now of 6 quantities, can be tamed. Analysis of the 2-point PDF may be more tractable than it seems, though, if the apparent near-Gaussianity of its copula (Scherrer et al. 2010) can be exploited. Applied to spatial statistics, the copula is a function giving all remaining information necessary to construct an N -point PDF from the 1-point PDF.

1.1 Density-dependent clustering

The statistic we introduce here, the sliced correlation function, is an integral over 1 instead of 2 of the densities in $f(\delta_1, \delta_2; r)$. Packaging the 2-point PDF into $\xi(r)$ gives something easily manageable, but at the cost of losing all sensitivity to non-Gaussian features.¹ Here, we explore going halfway: integrating $f(\delta_1, \delta_2; r)$ over only one density argument. The result retains sensitivity to physically interesting non-Gaussian effects, but is manageable enough for that sensitivity to be clearly visible.

Our particular formulation of sliced correlations is new, but they are not unrelated to previous investigations of how clustering depends on galaxy properties, such as density ('environment') and luminosity. Marked correlation functions weight pairs differently based on some property of each point (Illian et al. 2008; Szapudi et al. 2000; Faltenbacher et al. 2002; Sheth 2005; Sheth et al. 2005; Skibba et al. 2006). Density-marked correlation functions (White & Padmanabhan 2009; White 2016) are a bit in the spirit of sliced correlations, since changing the mark's dependence with density can probe low- and high-density regimes separately.

¹ Here we mean non-Gaussianity in the measured density field itself, not primordial non-Gaussianity, which can affect the ratio of the power spectrum of a biased tracer to the matter power spectrum (Dalal et al. 2008).

Note that density-marked correlation functions are similar to some higher-order statistics, two-point cumulant correlators (e.g. Szapudi & Szalay 1997), which measure two-point correlations of (usually positive integer) powers of δ .

Abbas & Sheth (2005, 2007) have also investigated density-dependent clustering, looking at autocorrelations of galaxies within different density contours, including some modeling that might be applied to sliced correlations. Pujol et al. (2015) have investigated some similar issues, looking at how scale-dependent halo bias depends on density. Also, Uhlemann et al. (2016) have developed a model, remarkably accurate into the mildly non-linear regime, of the 2-point PDF (where 'points' are spheres of some separation), which could be quite useful for modeling our results analytically. This model is based on spherical-collapse dynamics and the large-deviation principle (e.g. Bernardeau et al. 2014, 2015).

Another way to investigate density dependence is through analyzing voids (or clusters) separately, which has proven useful for cosmological analysis (e.g. Granett et al. 2008; Hamaus et al. 2016; Mao et al. 2016). There can be ambiguity in how to define a void (Colberg et al. 2008), but using the same definition in both mocks and observations eliminates that ambiguity. Still, our approach of sliced correlations may offer similar physical sensitivities as using voids and clusters, with arguably less ambiguity. Note that while here we slice correlations on the density itself, one can also slice on a function(al) of the density, e.g. a Mexican hat wavelet that quantifies the 'voidiness' on some scale at each position.

1.2 Shifts in the baryon acoustic feature

In this paper, we focus on how baryon acoustic oscillations (BAO) show up in sliced correlations, with features not visible in the usual correlation function. The BAO are a 'standard ruler' of great importance in measuring the cosmic expansion history (Eisenstein et al. 2005; Cole et al. 2005; Cuesta et al. 2016), and detecting them drives many current and future large-scale structure surveys.

One reason the BAO are so useful is that they are essentially linear-regime, $\sim 100 h^{-1}$ Mpc features. At low redshift, the peak remains nearly unmoved from its initial location in comoving coordinates, but other non-linearities are far from negligible. The largest non-linear effect is that flows on $\sim 10 h^{-1}$ Mpc scales broaden the feature in $\xi(r)$ (Crocce & Scoccimarro 2006). These flows are simple physically: in comoving coordinates, overdense regions contract, pulling the BAO peak inward, while underdense regions expand, pushing it outward (Sherwin & Zaldarriaga 2012; McCullagh et al. 2013). There is also a small shift in the BAO position (Smith et al. 2007; Seo et al. 2010) that these motions produce, because of the large weight that overdense regions get in the usual $\xi(r)$.

Lagrangian linear theory (the Zel'dovich approximation, ZA; Zel'dovich 1970) captures the shifting and smearing of the BAO simply and rather accurately, which is why it underlies the most widely used 'BAO reconstruction' methods (Eisenstein et al. 2007; Padmanabhan et al. 2012). In these methods, the BAO are reconstructed by estimating and removing the flows. Refinements of the method, going beyond ZA, have been proposed, as well (e.g. Mohayaee et al. 2006; Falck et al. 2012; Kitaura & Angulo 2012). Of particular relevance for the current paper, Achitouv & Blake (2015) have even looked at how this BAO reconstruction behaves for different local densities of galaxies.

Such reconstruction methods are perhaps the best way to sharpen the BAO feature for detection, but in practice they are quite involved. More importantly, they discard whatever information might be in the flows themselves. As we will see, the sliced

correlation function can extract this information, in a rather easily digested form.

2 DEFINITIONS

The definition of the usual correlation function is

$$\xi(r) = \langle \delta(\mathbf{x})\delta(\mathbf{x} + \mathbf{r}) \rangle = \iint \delta_1 \delta_2 f(\delta_1, \delta_2; r) d\delta_1 d\delta_2, \quad (1)$$

where $f(\delta_1, \delta_2; r)$ is the 2-point PDF, the joint distribution of densities δ_1 at $\delta(\mathbf{x})$, and δ_2 at $\delta(\mathbf{x} + \mathbf{r})$. The angled brackets here denote the expectation value. We assume isotropy here, so $\xi(r)$, the covariance of the distribution, is only a function of separation.

We introduce two related quantities. The *contour correlation function* $\varphi(r, \delta')$ is the cross-correlation of points in the density contour $\delta = \delta'$ with regions a distance r away from the contour:

$$\varphi(r, \delta') = \langle \delta(\mathbf{x} + \mathbf{r}) \rangle_{\delta(\mathbf{x})=\delta'} = \int \delta_2 f(\delta', \delta_2; r) d\delta_2. \quad (2)$$

Often, it is useful to bin densities logarithmically, as we do in this paper. This would change $d\delta$ to dA , where $A = \ln(1 + \delta)$.

The *sliced correlation function* is almost the same, except that inside the integral, the contour is weighted with its density. The sliced correlation function is

$$\xi(r, \delta') = \langle \delta(\mathbf{x})\delta(\mathbf{x} + \mathbf{r}) \rangle_{\delta(\mathbf{x})=\delta'} = \int \delta' \delta_2 f(\delta', \delta_2; r) d\delta_2. \quad (3)$$

For infinitesimal density bins, $\xi(r, \delta) = \delta \varphi(r, \delta)$. But a realistic measurement involves finite density bins. Explicitly using distance and density bins (r_i, δ_j) ,

$$\varphi(r_i, \delta_j) = \langle \delta(\mathbf{x} + \mathbf{r}) \rangle_{|\mathbf{r}| \in r_i, \delta(\mathbf{x}) \in \delta_j}, \quad (4)$$

$$\xi(r_i, \delta_j) = \langle \delta(\mathbf{x})\delta(\mathbf{x} + \mathbf{r}) \rangle_{|\mathbf{r}| \in r_i, \delta(\mathbf{x}) \in \delta_j}.$$

We focus on sliced correlation functions in this paper, but ξ and φ both have their advantages. $\xi(r, \delta)$ has a more direct interpretation for those familiar with $\xi(r)$: it is the contribution to $\xi(r)$ from density δ ,

$$\xi(r) = \int \xi(r, \delta) d\delta. \quad (5)$$

For $\xi(r, \delta)$, this sum can reconstruct the total $\xi(r)$ even with finite density bins; note that δ' is inside the integral in Eq. (3). The contour correlation function $\varphi(r, \delta)$ does not have this benefit, but it is sensitive to clustering even at the $\delta = 0$ contour, whereas $\xi(r, \delta = 0) = 0$, by definition.

While these definitions are unambiguous in principle, there are some practical choices to make when using $\xi(r, \delta)$. The full $\xi(r)$ can be measured directly from an unsmoothed field, but $\xi(r, \delta)$ depends on how the density is estimated (i.e., smoothed). This can be important, as we show below when slicing ξ with densities estimated with different smoothings. Density estimation can be with a fixed kernel (such as a Gaussian or top hat, which we use below), or with an adaptive method such as a Delaunay or Voronoi tessellation (Schaap & van de Weygaert 2000; van de Weygaert & Schaap 2009). With angular masks, and inhomogeneous sampling in the line-of-sight direction, estimating the density at each galaxy can be non-trivial. But as White (2016) points out, most modern surveys large enough for precision BAO measurement already incorporate a careful local-density estimate, for BAO-reconstruction purposes. Even using δ itself is a choice; a useful alternative could be a function of δ such as the log-density.

In this paper, we estimate $\xi(r, \delta)$ using a density field defined

on a fixed Eulerian grid, computing it with a fast Fourier transform (FFT) (Szapudi et al. 2005). In a pair-counting method, sliced correlations can be measured by binning pairs into a two-dimensional set of bins, of separation and the density of both points in the pair. The random pairs must then be scaled by the number of random pairs expected from the 1-point density PDF. Using a simple DD/RR estimator,

$$\xi(r, \delta) = DD(r, \delta) / [P(\delta)^2 RR(r)] - 1, \quad (6)$$

where $DD(r, \delta)$ is the number of data-data pairs where at least one of the points is in density bin δ and separation bin r , $RR(r)$ is the number of random-random pairs with separation r , and $P(\delta)$ is the fraction of particles in density bin δ .

The pair-counting and grid-FFT estimates of $\xi(r, \delta)$ should agree at large scales and high sampling, but there may be differences at scales smaller than interparticle spacings, since pair-counting only uses the density exactly at particles, whereas in a grid-FFT method, other locations are explicitly included. We plan to investigate any such differences in later work.

2.1 Gaussian field

For a zero-mean Gaussian field $\delta(\mathbf{x})$, the correlation function, including the zero-lag $\sigma^2 = \xi(r = 0)$, entirely determines $\xi(r, \delta)$. σ^2 depends on a smoothing, which we set to the same smoothing that is used for density slicing. In this case, for all r , $f(\delta_1, \delta_2; r)$ is a bivariate Gaussian distribution in δ_1 and δ_2 :

$$f(\delta_1, \delta_2; r) = \frac{1}{2\pi\sigma^2\sqrt{1-\varrho^2}} \exp\left[-\frac{\delta_1^2 + \delta_2^2 - 2\varrho\delta_1\delta_2}{2\sigma^2(1-\varrho^2)}\right], \quad (7)$$

where $\varrho(r) = \xi(r)/\sigma^2$ is the correlation coefficient of δ_1 and δ_2 . Putting this into Eq. (3) gives

$$\xi(r, \delta) = \frac{\delta^2 \varrho(r)}{\sqrt{2\pi}\sigma^2} \exp\left(-\frac{\delta^2}{2\sigma^2}\right). \quad (8)$$

In terms of the usual correlation function,

$$\xi(r, \delta) = \xi(r) \frac{\delta^2}{\sigma^3 \sqrt{2\pi}} \exp\left(-\frac{\delta^2}{2\sigma^2}\right). \quad (9)$$

For infinitesimal density bins, the contour correlation function $\varphi(r, \delta) = \xi(r, \delta)/\delta$:

$$\varphi(r, \delta) = \xi(r) \frac{\delta}{\sigma^3 \sqrt{2\pi}} \exp\left(-\frac{\delta^2}{2\sigma^2}\right). \quad (10)$$

Note that in this Gaussian case, $\varphi(r, \delta = 0) = 0$, but not in general for a non-Gaussian field.

Fig. 1 shows an example of $r^2 \xi(r, \delta)$ for a Gaussian random field with a fiducial Λ CDM linear-theory $\xi(r)$, smoothed with a 3D Gaussian filter with $\sigma = 3 h^{-1}$ Mpc. The left panel shows a cross-section at fixed r ; it has a symmetric, bimodal shape, with peaks at $\delta = \pm \sigma \sqrt{2}$.

3 SLICED CORRELATIONS IN SIMULATIONS

The sliced correlations we show are averaged from 218 N -body simulations in the Indra suite (Falck et al., in prep). Each simulation, run with GADGET2 (Springel 2005), has side length $1 h^{-1}$ Gpc, with 1024^3 particles, assuming a Λ CDM cosmology: $(\Omega_m, \Omega_\Lambda, \Omega_b, h, \sigma_8, n_s) = (0.272, 0.728, 0.045, 0.704, 0.81, 0.967)$.

We measured the sliced correlation function $\xi(r, \delta)$ in

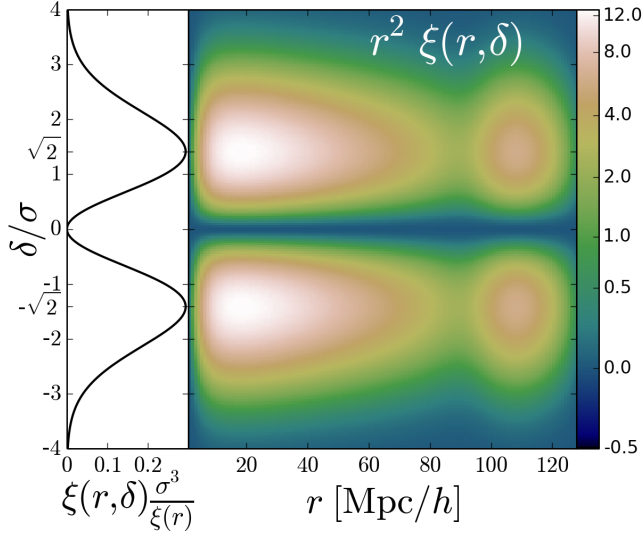


Figure 1. **Right:** $r^2 \xi(r, \delta)$ for a linear-theory Λ CDM Gaussian random field, as given in Eq. (9). The BAO feature comes out as blobs at the peak scale of $\sim 108 h^{-1}$ Mpc, at the base of each sideways exclamation mark. Note the nonlinear (\sinh^{-1}) colour scale; it goes negative for similarity to later plots, but the quantity plotted remains non-negative. **Left:** a cross-section at fixed r . For a Gaussian field, this shape is independent of r .

each δ bin by computing the cross-correlation of $\delta(\mathbf{x})$ with $[\delta(\mathbf{x})\{\delta(\mathbf{x}) \in \delta_j\}]$, using an FFT. Here, $\{\delta(\mathbf{x}) \in \delta_j\}$ is 1 if $\delta(\mathbf{x})$ is in the density bin δ_j , and 0 if not. This is computationally efficient if the number of density bins δ_j is small, but the computational time scales with the number of δ_j . A pair-counting estimator could be more efficient than this FFT method, for a large number of density bins.

Fig. 2 shows the real-space, dark-matter $\xi(r, \delta)$ averaged from these simulations. In the first panel, we divide each row by dA , the interval in $A = \ln(1 + \delta)$. Thus, the total $\xi(r)$ can be reconstructed by summing up vertically. The density was estimated on a grid of 512 cells of size $\frac{1000}{512} \approx 2 h^{-1}$ Mpc, using cloud-in-cell (CIC) interpolation. The density bins are logarithmic in $(1 + \delta)$, the right axis showing the log-density $A = \ln(1 + \delta)$ in units of its dispersion σ_A . In the second panel, we enhance the contrast of the BAO peak in each δ bin, normalizing $\xi(r, \delta)$ to 0 at the minimum near $85 h^{-1}$ Mpc, and 1 at the peak near $108 h^{-1}$ Mpc.

Two differences from the Gaussian case are evident here, i.e. non-Gaussianities that $\xi(r, \delta)$ is sensitive to.

First, the full $\xi(r)$ signal is distributed among the density bins differently than in the Gaussian case. High densities greatly dominate, the contribution peaking around $\delta \sim 20$. Panel 3 shows that the contribution from $\delta < 0$ (dashed) is an order of magnitude smaller than from $\delta > 0$ (dotted). There is even a region with slightly negative δ which contributes negative signal to $\xi(r)$; that is, with $\xi(r, \delta)/\xi(r) < 0$, a qualitative departure from the Gaussian case. We are not the first to see this sort of effect; Abbas & Sheth (2007) found observationally that modestly underdense galaxies in the Sloan Digital Sky Survey are negatively correlated to the rest of the field. Also, consistent with our results, Uhlemann et al. (2016) found that in the low- z matter density field, the δ with zero ‘bias’ (correlation) is slightly negative; they also provided a perturbative estimate of the offset from zero.

How should we understand this ‘valley of negativity?’ Suppose that δ is a local monotonic biasing transform b of a Gaus-

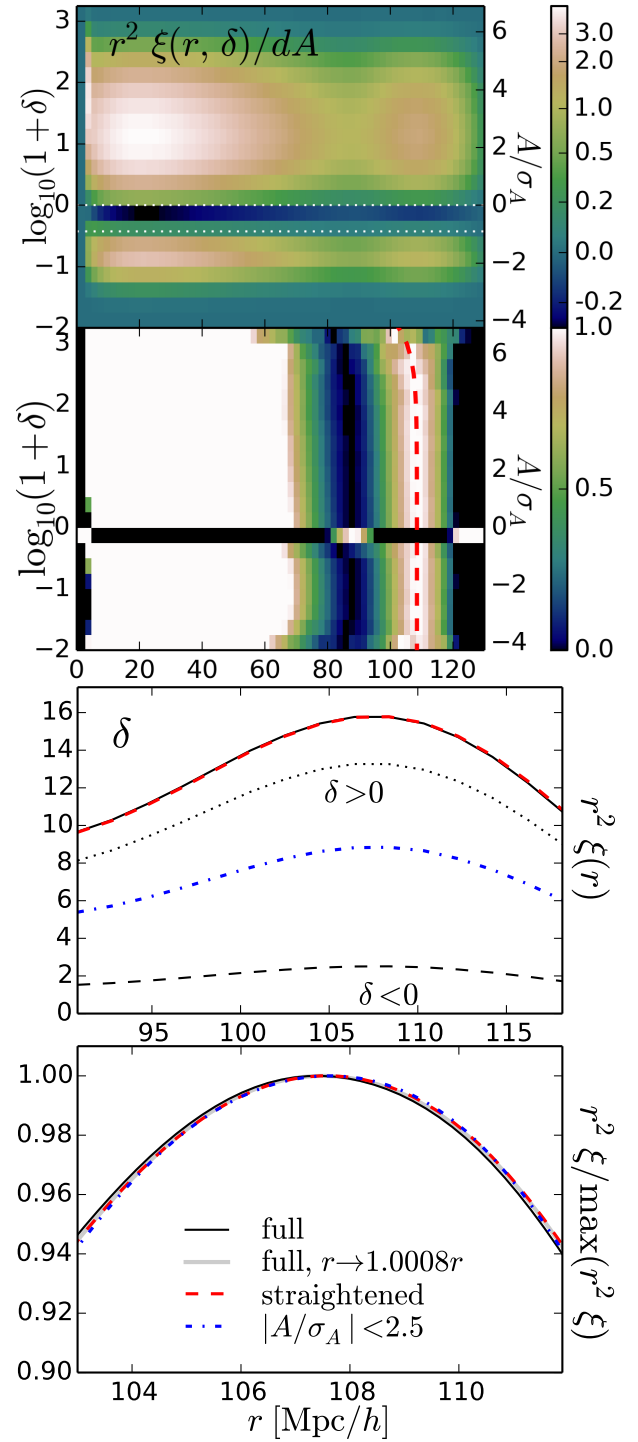


Figure 2. **(1, top)** The sliced correlation function $r^2 \xi(r, \delta)$ as measured from simulations. Dotted white lines show the mean and median density. Note the non-linear colourscale. **(2)** $r^2 \xi(r, \delta)$, enhanced to show the BAO peak location separately in each δ bin. A dashed red curve shows a by-eye fit to the peak location in each bin, given by Eq. (11). **(3)** The total $r^2 \xi(r)$ (solid black), and partial sums of $r^2 \xi(r, \delta)$: only $\delta > 0$ (dotted); only $\delta < 0$ (dashed), and bins with $A = \ln(1 + \delta)$ within 2.5σ of 0 (dotdashed blue). The red dotted curve has been ‘straightened,’ i.e. $\xi(r, \delta)$ is scaled in each δ bin to straighten the dashed fit in panel 2. **(4, bottom)** These curves, spline-interpolated, and normalized to unity at their maximum. The gray curve is meant to show peak motion from black to dashed red, scaling r by the factor shown. The various curves are clearer in Fig. 3, which has bigger shifts.

sian field G , $\delta = b(G)$. $\xi(\delta, r)$ generally has two classes of zero-crossings: where $\delta = 0$ (by definition), but also where $\phi(\delta, r) = 0$. In our measurements, $\phi(\delta, r) = 0$ near the *median*, not mean ($\delta = 0$) density. In the $\delta = b(G)$ model, b transforms mean-density regions of the Gaussian G to the median density of δ , so in δ , median-density regions are clustered like mean-density regions of a Gaussian field. Between these zeroes at the mean and median, $\xi(\delta, r)$ generally goes negative. The behaviour of $\xi(\delta, r)$ as δ varies at fixed r seems driven by the non-Gaussianity of the 1-point PDF. Indeed, we expect departures from the Gaussian $\xi(r, \delta)$ to increase as the density is smoothed on smaller scales, giving a more non-Gaussian 1-point PDF. We plan to explore this behaviour in an upcoming paper.

3.1 BAO peak motions with small-scale density

The second interesting non-Gaussianity, which we focus on here, is the inward motion of the BAO at high density. This effect has a clear physical origin: a patch exceeding the mean density contracts in comoving coordinates, while an underdense patch expands in comoving coordinates.

However, this effect is quite small in Fig. 2, only clearly evident in the densest bin. This is because it is the density on scales comparable to the BAO scale, $\sim 100 h^{-1}$ Mpc, that drive the feature in or out, while here, we slice on the density estimated on only $2 h^{-1}$ Mpc scales. This $2 h^{-1}$ Mpc density is only weakly correlated with the density on $100 h^{-1}$ Mpc scales, but evidently is correlated enough that the highest $2 h^{-1}$ Mpc densities tend to be in BAO-scale overdensities, that contract. There is also a suggestion of inward motion in the lowest-density bin, which may be from noise.

In the red dashed curve, we show a by-eye fit to the dependence of the peak location on density. We formulate it in terms of a scaling factor

$$s(\delta) = 1 - s_\delta \delta - s_A \ln(1 + \delta), \quad (11)$$

where s_δ and s_A are constants. In Fig. 2, $(s_\delta, s_A) = (3 \times 10^{-5}, 0)$. s_A is nonzero in the next such fit.

In the bottom two panels, we zoom in on the BAO feature and show partial sums of $\xi(r, \delta)$. The dashed red curve is a ‘straightened’ $\xi_{\text{straight}}(r) = \int \xi(s(\delta)r, \delta) d\delta$. This lines up the BAO at the same scale, under the assumption that the comoving expansion or contraction at $\delta \neq 0$ scales $\xi(r, \delta = 0)$ with the factor $s(\delta)$. When totaling up ξ_{straight} , we scaled $\xi(r, \delta)$ by linear interpolation in r . Comparing ξ_{straight} to the full, raw $\xi(r)$ allows an estimate of how much the flows in different density regimes shift the total peak location. To measure how much of the BAO shift can be undone in principle with this straightening, we show $\xi(r)$, with r scaled by a factor of 1.0008. This is an order of magnitude less than the full $\sim 0.6\%$ shift described below; thus, it appears that slicing the correlation function on a small-scale density estimate captures little of the flows we are after.

The blue dot-dashed curve excludes only $> 2.5\sigma$ extremes of the log-density distribution, which also partially restores the peak position. In effect, clipping these extremes in the tail of the distribution out of the summed $\xi(r)$ is similar to clipping the density field (Simpson et al. 2011), a technique which brings low-order statistics into better agreement with perturbative predictions, and reduces covariances, providing similar benefits as Gaussianization. (In our case, clipping out cross-correlations from the total $\xi(r)$ differs from clipping the field itself; in that case, pixels over the threshold remain fully in the sample, but with a density set to the clipping

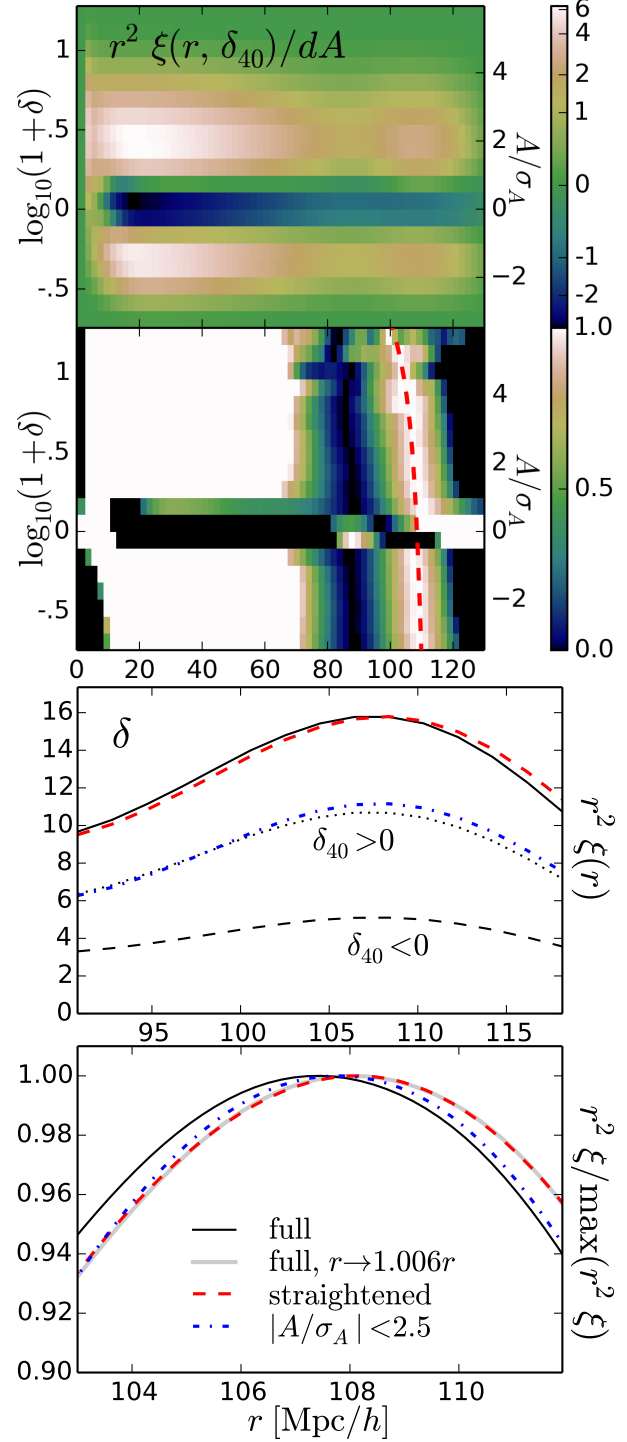


Figure 3. The same as in Fig. 2, except slicing on δ_{40} , which is δ smoothed with a $40 h^{-1}$ Mpc real-space-top-hat filter.

threshold.) Thus, it seems that as with a logarithmic transform (McCullagh et al. 2013), the reduction of the shift in the BAO peak position is another benefit of clipping. There is ambiguity in where to place the clipping threshold, but a practical approach would be to clip to a level that brings systematic errors within the statistical errors.

3.2 BAO peak motions with larger-scale densities

Would slicing on a larger-scale density estimate enhance the motions revealed in $\xi(r, \delta)$? In Fig. 3, we slice on δ_{40} , δ smoothed with a Gaussian of $\sigma = 40 h^{-1}$ Mpc. The dependence of the peak position with radius is much stronger here. The fit to the peak motion has correspondingly larger coefficients: $(s_\delta, s_A) = (3 \times 10^{-3}, 6 \times 10^{-3})$. The bottom panels of Fig. 3 show that straightening the dashed red fit to the BAO peak motion results in a much larger shift, corresponding remarkably well with the inward shift by 0.5%-0.6% in the real-space matter correlation function at $z = 0$ found by Seo et al. (2010).

Clipping out $> 2.5\sigma$ tails of the distribution from the summed $\xi(r)$ also partially restores the peak position, but not as much as ‘straightening.’ We did not experiment with this threshold; doing so would have limited value without also considering the noise. As the threshold is brought to $\delta = 0$, we would expect the peak position to be increasingly unbiased, but at the expense of increasing variance, as the volume used for analysis is decreased.

While we have enhanced the BAO motions with the larger filter, we have also exposed some curiosities. The ‘valley of negativity’ where $\xi(r, \delta)/\xi(r) < 0$ has become more complex. We attribute this complexity to the difference between the field sliced on, and the field that slices are cross-correlated with, which is still δ CIC-estimated in $2 h^{-1}$ Mpc cells. Also, unfortunately, there is still disappointingly little BAO-peak motion evident for $\delta_{40} < 0$.

If the motion of the peak is enhanced with a $40 h^{-1}$ Mpc filter, what happens with a BAO-scale, $\sim 100 h^{-1}$ Mpc filter, that would entirely capture the regions undergoing contraction or expansion with density? Unfortunately, slicing on such a large-scale-smoothed density gives some curious results.

Fig. 4 shows $\xi(r, \delta_{100})$, slicing on δ_{100} , δ smoothed with a top hat of radius $100 h^{-1}$ Mpc. Bizarrely, there is no visible BAO peak in any density slice. Instead, the main effect of slicing with δ_{100} seems to be the sharp cliff at the edge of the top hat, at $100 h^{-1}$ Mpc; this is evidently just the average density profile of a peak or trough in δ_{100} . The intermediate density bins do have peaks at $r \sim 115 h^{-1}$ Mpc, but they may be related not to BAO, but to the peak and trough profiles being carved out of the total $\xi(r)$.

The full run of $\xi(r, \delta_{100})$ with δ_{100} seems difficult to interpret, but a simple split at $\delta < 0$ and $\delta > 0$ gives interesting and promising results. As the bottom panel of Fig. 4 shows, there seems to be a substantial shift in the BAO position, by up to $\sim 5 h^{-1}$ Mpc, in this ‘split correlation function.’

Also, interestingly, the BAO peak has a bit higher amplitude in overdense regions; the 1-point PDF of δ_{100} is Gaussian enough ($\delta_{\text{median}} = -0.003\sigma$) that this is another clear non-Gaussian feature. This may indicate some thinning and sharpening of the BAO shell itself, or an increased growth rate, in overdense regions. Applied to galaxies, the peak heights in overdense and underdense regimes may also hold information about halo bias.

We also did try a $50 h^{-1}$ Mpc Gaussian smoothing, giving some features reminiscent of the complex $100 h^{-1}$ Mpc top-hat result at the highest densities. Understanding and optimizing how the density is sliced (the filter, the number of slices, etc.) is an obvious further avenue for work.

4 CURTAIN PLOTS OF DENSITY-DEPENDENT FLOWS

Knowing the initial and final conditions of a simulation, it is possible to measure how much motion we could hope to capture in

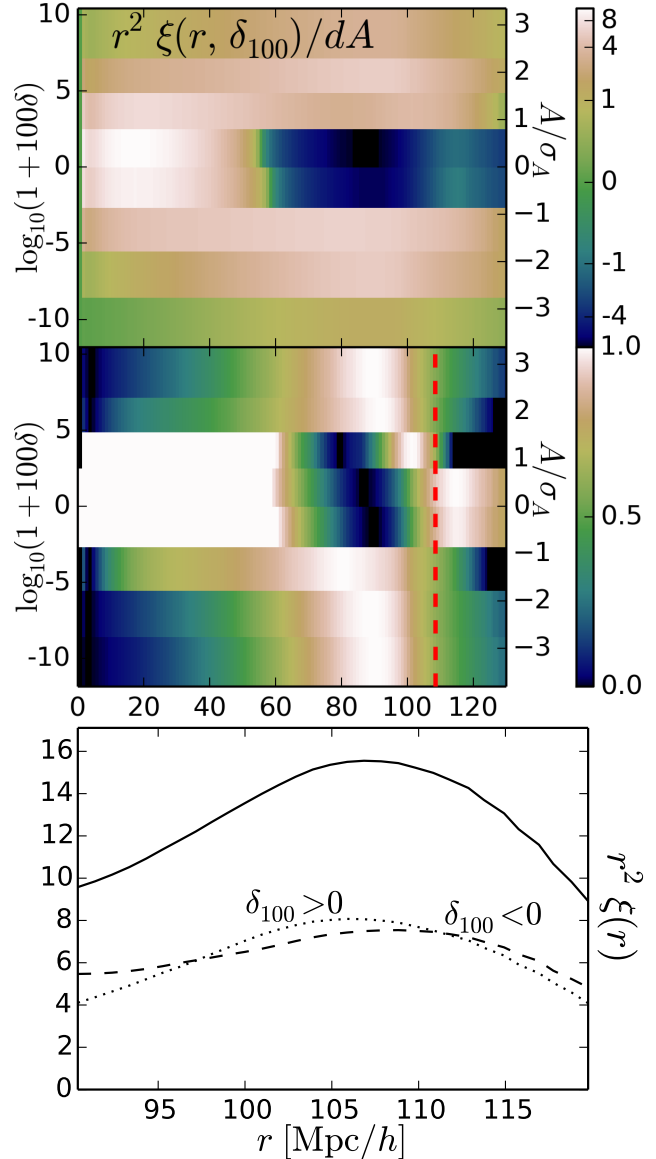


Figure 4. Similar to Figs. 2 and 3, except slicing on δ_{100} , i.e. δ smoothed with a $100 h^{-1}$ Mpc real-space-top-hat filter. The red dashed line in the middle panel is simply a straight vertical line at the same radius as in previous such plots, with no attempt at fitting the ‘BAO peak.’ At the extremes in δ , peaks seem to come from the average profiles of regions with particular top-hat densities, not from the BAO. However, in the bottom panel, a substantial difference is noticeable between underdense and overdense regions, as defined by δ_{100} .

principle with sliced or contour correlations, in the unrealistic case that there were some marker like the BAO at each radius. ‘Curtain plots’ appear in Fig. 5, showing how the average radial motion of matter shells around particles in an N -body simulation depends on the central particles’ initial local density. More directly relevant to sliced correlations (sliced according to the final density) would be a measurement of how these motions depend on the final density. But this measurement would be dominated by the trivial effect that in the final conditions, a high-density region is by definition produced by substantial inward flows.

To make the plot, we averaged final separations r_{Eul} between pairs of particles in each $(r_{\text{Lag}}, \delta_{\text{Lag}})$ bin, i.e., bins $(4 h^{-1} \text{ Mpc})$

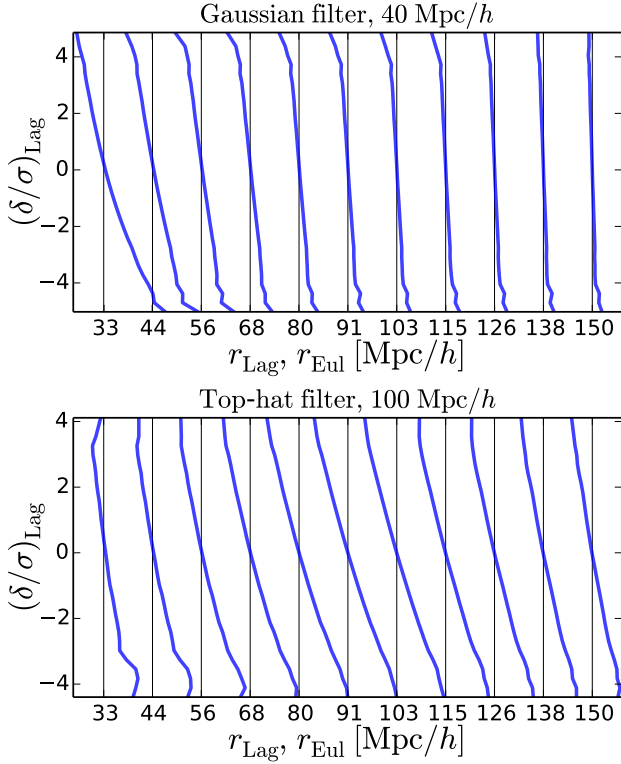


Figure 5. ‘Curtain’ plots showing the average inward or outward motion of shells around particles from the initial conditions to $z = 0$, as a function of the initial density δ_{Lag} of the particles, and the initial radii of the shells, r_{Lag} . Thin black lines show the initial radii of the shells, and thick blue curves show the average separation between the particle with density on the y -axis and particles initially in the shell. The labels above the panels describe the filters applied to δ_{Lag} , along the y -axis. On average, shells around extreme $100 h^{-1}$ Mpc-top-hat-smoothed regions move by over $10 h^{-1}$ Mpc.

wide) of initial separation, and initial density of one of the particles. We used a 512^3 -particle simulation with the same box size as those used above; only one simulation was necessary for a good measurement, given initial particle positions. The thin, vertical lines show shell radii in the initial conditions, before the particles move. The thick curves, one per initial radius r_{Lag} bin, show the final-conditions average distance to these particles (i.e., the final average radii of the shells). In underdense regions (at the bottom of the plots), particles move away from each other on average, and thus have greater Eulerian than Lagrangian separation. Likewise, in overdense regions, particles move toward each other on average, producing a smaller Eulerian than Lagrangian separation.

Unsurprisingly, the scale used for filtering is the scale at which motions are best picked up. In the top panel, the thick lines are most slanted at $\sim 40 h^{-1}$ Mpc, getting more vertical at smaller and larger r . Similarly, in the bottom panel, the thick lines are most slanted at $\sim 100 h^{-1}$ Mpc. Motions on other scales happen because of correlations between densities filtered on those scales and the scale used for the filter. The slanted lines are more symmetric in over- and underdense regions than the BAO peaks in sliced correlations show; perhaps this is related to the initial rather than final densities used for binning here.

5 CONCLUSION

We introduce the sliced correlation function, a two-point statistic that measures density-dependent clustering. It is sensitive to several physically interesting effects that the usual correlation function misses, but we focus attention here on shifts with density of the baryon acoustic oscillation (BAO) feature.

The density-dependent motions of the BAO peak come out clearly: it moves by up to $\sim 10 h^{-1}$ Mpc for the highest-density peaks, when smoothing on a $40 h^{-1}$ Mpc scale. These motions are sensitive to cosmological parameters: in the Zel’dovich approximation, they are exactly scaled with the growth factor (sensitive to parameters like σ_8 , Ω_M , and w). Since the sliced correlation function measures density-dependent clustering, it should be sensitive to modified gravity models that deviate from general relativity only in regions of low density or low gravitational potential (for a review, see Joyce et al. 2015). The full sliced correlation function likely has this sensitivity, but it would likely be most detectable in the density-dependent shift of the BAO peak.

We have shown examples of sliced correlation functions sensitive to BAO peak motions. Slicing on a $40 h^{-1}$ Mpc-filtered density gives a sliced correlation function sensitive to the complete run of BAO peak position with density. Slicing on a $100 h^{-1}$ Mpc-filtered density, on the other hand, seems to be useful mainly when splitting the sample into very wide slices (positive and negative δ_{100}). Conveniently, these filters are large enough to expect observational effects such as galaxy discreteness and bias to be manageable. Still, careful modeling will be necessary for precision analysis.

There is much room for further study of density-dependent BAO analysis. We need to investigate how to optimize the detection of peak motions, in light of observational effects. Here, we have glossed over error bars, but preliminarily, we have found that sliced correlations of a 1-point-Gaussianized density field have increased S/N in each bin. Another question is how many slices to make. The fully sliced $\xi(r, \delta)$ could be most information-rich in principle, but it may be most convenient and powerful to analyze a single function, or small set of functions. It also may be useful to estimate the peak location and strength at each location (Arnalte-Mur et al. 2012), using a wavelet method (see also Xu et al. 2010; Tian et al. 2011; Labatie et al. 2012). Looking at how the wavelet coefficients vary with density may offer a way to estimate peak motions without explicit density binning.

The sliced correlation function has many other applications which we plan to explore. A curious feature is a ‘valley of negativity,’ at slightly negative δ , which subtracts signal from the total correlation function. This could relate to loss of information in the usual correlation function, since we preliminarily find that the valley of negativity disappears when measuring the sliced correlation function of the 1-point-Gaussianized density (known to be more information-rich in general). The complete run of $\xi(r, \delta)$ with δ seems related to the 1-point PDF; because biasing also alters the 1-point PDF, sliced correlations may help to understand the bias of galaxies or other tracers. In redshift space, sliced correlations may be useful to understand or work around fingers of god, which corrupt low-density regions less than the high-density regions that dominate the usual correlation function.

ACKNOWLEDGMENTS

We thank Ravi Sheth for helping to spark this particular project with a suggestion to scale pairs according to local density (for the

purpose of BAO-peak sharpening), and for helpful comments on a draft of the paper. We also thank Marius Cautun and Shaun Cole for useful discussions. MN and NM were supported at Durham by the UK Science and Technology Facilities Council (ST/L00075X/1) and the European Research Council (DEGAS-259586). MN was supported at IAP under the ILP LABEX (ANR-10-LABX-63) supported by French state funds managed by the ANR within the Investissements d’Avenir programme under reference ANR-11-IDEX-0004-02, and also by ERC Project No. 267117 (DARK) hosted by Universit  Pierre et Marie Curie (UPMC) Paris 6, PI J. Silk. MN and AS were supported at JHU by a grant in Data-Intensive Science from the Gordon and Betty Moore and Alfred P. Sloan Foundations. IS acknowledges support by NASA grants NNX12AF83G and NNX10AD53G, and NSF grant AST-1616974. BF acknowledges financial support from the Research Council of Norway (Programme for Space Research). JW was supported by NSFC grants 11390372 and 11373029, and the Pilot-B project.

REFERENCES

- Abbas U., Sheth R. K., 2005, *MNRAS*, 364, 1327
- Abbas U., Sheth R. K., 2007, *MNRAS*, 378, 641
- Achitouv I., Blake C., 2015, *Phys. Rev. D*, 92, 083523
- Aitchison J., Brown J. A. C., 1957, *The Lognormal Distribution*. Cambridge University Press, Cambridge
- Arnalte-Mur P., Labatie A., Clerc N., Mart nez V. J., Starck J.-L., Lach  ze-Rey M., Saar E., Paredes S., 2012, *A&A*, 542, A34
- Bernardeau F., Pichon C., Codis S., 2014, *Phys. Rev. D*, 90, 103519
- Bernardeau F., Codis S., Pichon C., 2015, *MNRAS*, 449, L105
- Carron J., 2011, *ApJ*, 738, 86
- Carron J., Neyrinck M. C., 2012, *ApJ*, 750, 28
- Carron J., Szapudi I., 2014, *MNRAS*, 439, L11
- Colberg J. M., et al., 2008, *MNRAS*, 387, 933
- Cole S., et al., 2005, *MNRAS*, 362, 505
- Coles P., Jones B., 1991, *MNRAS*, 248, 1
- Crocce M., Scoccimarro R., 2006, *Phys. Rev. D*, 73, 063520
- Cuesta A. J., et al., 2016, *MNRAS*, 457, 1770
- Dalal N., Dor  O., Huterer D., Shirokov A., 2008, *Phys. Rev. D*, 77, 123514
- Eisenstein D. J., et al., 2005, *ApJ*, 633, 560
- Eisenstein D. J., Seo H.-J., Sirko E., Spergel D. N., 2007, *ApJ*, 664, 675
- Falck B. L., Neyrinck M. C., Szalay A. S., 2012, *ApJ*, 754, 126
- Faltenbacher A., Gottl ber S., Kerscher M., M ller V., 2002, *A&A*, 395, 1
- Granett B. R., Neyrinck M. C., Szapudi I., 2008, *ApJL*, 683, L99
- Hamaus N., Pisani A., Sutter P. M., Lavaux G., Escoffier S., Wandelt B. D., Weller J., 2016, *Physical Review Letters*, 117, 091302
- Hill J. C., et al., 2014, preprint, (arXiv:1411.8004)
- Illian J., Penttinen P., Stoyan H., Stoyan D., 2008, *Statistical Analysis and Modelling of Spatial Point Patterns*. Statistics in Practice, Wiley, https://books.google.co.uk/books?id=_U6BER2stYsC
- Joyce A., Jain B., Khoury J., Trodden M., 2015, *Phys. Reports*, 568, 1
- Kitaura F.-S., Angulo R. E., 2012, *MNRAS*, 425, 2443
- Labatie A., Starck J. L., Lach  ze-Rey M., 2012, *ApJ*, 746, 172
- Liu J., Hill J. C., Sherwin B. D., Petri A., B hm V., Haiman Z., 2016, preprint, (arXiv:1608.03169)
- Mao Q., Berlind A. A., Scherrer R. J., Neyrinck M. C., Scoccimarro R., Tinker J. L., McBride C. K., Schneider D. P., 2016, preprint, (arXiv:1602.06306)
- McCullagh N., Neyrinck M. C., Szapudi I., Szalay A. S., 2013, *ApJL*, 763, L14
- McCullagh N., Neyrinck M., Norberg P., Cole S., 2016, *MNRAS*, 457, 3652
- Mohayaee R., Mathis H., Colombi S., Silk J., 2006, *MNRAS*, 365, 939
- Neyrinck M. C., 2014, in Heavens A., Starck J.-L., Krone-Martins A., eds, *IAU Symposium Vol. 306, Statistical Challenges in 21st Century Cosmology*. pp 251–254 (arXiv:1407.4815), doi:10.1017/S1743921314013702
- Neyrinck M. C., Szapudi I., 2007, *MNRAS*, 375, L51
- Neyrinck M. C., Szapudi I., Rimes C. D., 2006, *MNRAS*, 370, L66
- Neyrinck M. C., Szapudi I., Szalay A. S., 2009, *ApJL*, 698, L90
- Padmanabhan N., Xu X., Eisenstein D. J., Scalzo R., Cuesta A. J., Mehta K. T., Kazin E., 2012, *MNRAS*, 427, 2132
- Planck Collaboration et al., 2014, *A&A*, 571, A24
- Pujol A., Hoffmann K., Jim nez N., Gazta aga E., 2015, preprint, (arXiv:1510.01692)
- Repp A., Szapudi I., Carron J., Wolk M., 2015, *MNRAS*, 454, 3533
- Rimes C. D., Hamilton A. J. S., 2005, *MNRAS*, 360, L82
- Rimes C. D., Hamilton A. J. S., 2006, *MNRAS*, 371, 1205
- Schaap W. E., van de Weygaert R., 2000, *A&A*, 363, L29
- Scherrer R. J., Berlind A. A., Mao Q., McBride C. K., 2010, *ApJL*, 708, L9
- Seo H.-J., et al., 2010, *ApJ*, 720, 1650
- Sherwin B. D., Zaldarriaga M., 2012, *Phys. Rev. D*, 85, 103523
- Sheth R. K., 2005, *MNRAS*, 364, 796
- Sheth R. K., Connolly A. J., Skibba R., 2005, *ArXiv Astrophysics e-prints*,
- Simpson F., James J. B., Heavens A. F., Heymans C., 2011, *Physical Review Letters*, 107, 271301
- Skibba R., Sheth R. K., Connolly A. J., Scranton R., 2006, *MNRAS*, 369, 68
- Smith R. E., Scoccimarro R., Sheth R. K., 2007, *Phys. Rev. D*, 75, 063512
- Springel V., 2005, *MNRAS*, 364, 1105
- Szapudi I., Szalay A. S., 1997, *ApJL*, 481, L1
- Szapudi I., Branchini E., Frenk C. S., Maddox S., Saunders W., 2000, *MNRAS*, 318, L45
- Szapudi I., Pan J., Prunet S., Budav ri T., 2005, *ApJL*, 631, L1
- Takada M., Jain B., 2009, *MNRAS*, 395, 2065
- Takahashi R., et al., 2011, *ApJ*, 726, 7
- Tian H. J., Neyrinck M. C., Budav ri T., Szalay A. S., 2011, *ApJ*, 728, 34
- Uhlemann C., Codis S., Kim J., Pichon C., Bernardeau F., Pogossyan D., Park C., L’Huillier B., 2016, preprint, (arXiv:1607.01026)
- White S. D. M., 1979, *MNRAS*, 186, 145
- White M., 2016, preprint, (arXiv:1609.08632)
- White M., Padmanabhan N., 2009, *MNRAS*, 395, 2381
- Wolk M., Carron J., Szapudi I., 2015, *MNRAS*, 454, 560
- Xu X., et al., 2010, *ApJ*, 718, 1224
- Zel’dovich Y. B., 1970, *A&A*, 5, 84
- van de Weygaert R., Schaap W., 2009, in Mart nez V. J., Saar E., Mart nez-Gonz lez E., Pons-Border a M.-J., eds, *Lecture Notes in Physics, Berlin Springer Verlag Vol. 665, Data Analysis in Cosmology*. pp 291–413, doi:10.1007/978-3-540-44767-2_11